Far-infrared EPR of $Al_2O_3:Mn^{3+}$ and γ-irradiated ruby

R. L. Aurbach and P. L. Richards

Department of Physics, University of California, and Inorganic Materials Research Division, Lawrence Berkeley Laboratory, Berkeley, California 94720

(Received 5 May 1975)

The far-infrared spectra of four samples of Mn-doped Al_2O_3 were measured in the frequency range from 3 to 30 cm^{-1} in applied magnetic fields up to 55 kG using the techniques of Fourier-transform spectroscopy. Several absorption lines, which are attributed to Mn^{3+} ions, were observed for fields oriented both parallel and perpendicular to the c axis. Polarization measurements established that the lines were due to electric dipole transitions. The temperature dependence of the lines was studied in the range from 1.3 to 20 K. Both ground- and excited-state transitions were studied. The ground state was found to be a singlet. Ground-state transition intensities were found to be magnetic field dependent. A crystal-field theory was developed which successfully describes the low-lying states. The Jahn-Teller interaction, which is known to be important for this ion, is included in the theory only in the approximation that its effect is to quench the strengths of various terms in the Hamiltonian. The empirically determined trigonal field and spin-orbit quenching parameters are approximately 0.6 and 0.1, respectively. Excellent agreement with experiment was obtained for the ground-state transitions. The less good agreement obtained for excited-state transitions reveals weaknesses in the model. A γ-irradiated ruby was also studied and very weak absorption lines believed due to Cr^{2+} and Cr^{4+} were observed.

I. INTRODUCTION

One of the subjects of continuing interest in the study of dilute transition-metal ions in crystals has been systems with orbitally degenerate ground states, in which the Jahn-Teller (JT) effect plays an important role. An example is the ^5E ground state of the isoelectronic species Mn^{3+} and Cr^{2+} in Al_2O_3. Previous experimental work on these ions has principally involved measurements of thermal conductivity[1,2] and acoustic paramagnetic resonance.[3-6] Some preliminary infrared measurements have also been reported.[7,8] In this paper we report the results of a detailed study of the far-infrared spectrum of Mn^{3+} in Al_2O_3.

In order to describe our data, we have developed a phenomenological model for the low-lying states of Mn^{3+} in Al_2O_3 based on a crystal-field Hamiltonian in the absence of the JT interaction. The strengths of the crystal-field terms are adjusted to fit the data. We find that various parameters have smaller values than anticipated for a purely electronic Hamiltonian. We interpret this quenching as due to the effect of the JT interaction. An overview of the model may be obtained using simple group-theoretic arguments. The model will be described in detail later.

The Mn^{3+} ion is believed to enter Al_2O_3 at substitutional Al^{3+} sites which have site symmetry C_3. The crystal field at such a site is predominantly cubic with a trigonal distortion. As is shown in Fig. 1(a), the free-ion $(3d^4)\,^5D$ Hund's-rule ground state of Mn^{3+} is split by the cubic field into $^5E + {}^5T_2$, with ^5E lower. The trigonal field splits the $^5T_2$ state, but leaves the ^5E level degenerate. This degeneracy is lifted by the spin-orbit interaction in second order, and by the spin-spin interaction in first order.

In Fig. 1(b) we show the splitting of the ^5E ground state in more detail. Early crystal-field calculations,[3] which did not allow for the quenching of the trigonal field, predicted that the lowest-lying ^5E level was a doublet. Following a suggestion by Bates we consider a strongly quenched trigonal field. Applying first the spin-orbit and spin-spin interactions to the ^5E level of Mn^{3+} in a cubic field, five equally spaced levels with separation δ result. The lowest level is a singlet. In order of increasing energy the other levels are a triplet, a doublet, a triplet, and a singlet. The trigonal field splits each triplet into a doublet and a singlet and slightly changes the level splittings. If the trigonal field were not quenched, the singlet split off from the lowest triplet would be degenerate with the ground singlet. Our data show that the lowest level of the system is in fact a singlet. For purposes of discussion it will be convenient to label the energy levels as is indicated by the numbers on the right-hand side of Fig. 1(b). This is the order of the levels in the absence of an applied magnetic field.

II. EXPERIMENTAL DETAILS

The results described in this paper were obtained using Fourier-transform spectroscopy in a conventional transmission geometry which has been described in detail elsewhere.[9,10] Most of the measurements were made with a polarizing Michelson interferometer (PMI). This type of instrument, first proposed by Martin and Puplett,[11] uses a linear-grid polarizer, made of free-standing wires,

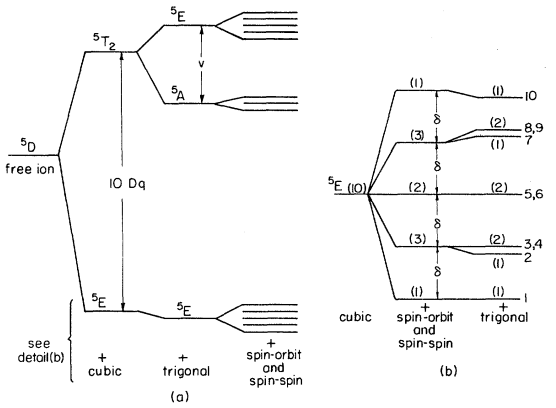

FIG. 1. Schematic energy-level diagram of a $(3d^4)\ ^5D$ term in Al_2O_3. Note that, although the trigonal field has a large role in the excited state splittings (a), it enters only in higher order in the splittings of the ^5E ground state (b). The numbers in parentheses indicate level degeneracies. The numbers on the right-hand side of the figure indicate a numbering scheme used to refer to the states.

as a beamsplitter. In practice, the use of this type of beamsplitter has been found to result in a significant improvement in low-frequency (< 10 cm^{-1}) performance compared with a conventional Michelson interferometer with a Mylar beamsplitter. The PMI constructed for these experiments was based on a modified "cube" interferometer obtained from H. A. Gebbie.

The samples were wrapped in thin Al foil to minimize the radiation losses out the sides and thus form a low-Q transmission cavity. They were then mounted in a cryostat at the center of a 55-kG superconducting solenoid. Radiation was coupled into and out of the sample using conical light concentrators. Radiation transmitted by the samples was detected using a helium-temperature doped-Ge bolometer. Its output was synchronously detected, digitized, and stored online in a PDP 11 computer. The computer was programmed to handle data acquisition and display, to Fourier transform the data to obtain spectra in real time, and to perform first-order data analysis. The instrumental response function was removed by computing ratios of pairs of spectra as is shown in Fig. 2(a). The peak at 9.35 cm^{-1} is due to an absorption line in the zero-field denominator. The other features, marked by solid arrows, are due to absorption lines in the numerator.

The four samples used in this work were obtained from the sources indicated in Table I. Spectrochemical analyses were made in order to identify the impurity responsible for the observed absorption lines. By comparing the observed line strengths in different samples with the respective spectrochemical analyses, it is possible to rule out all likely sources of the lines, except Mn^{3+}.

III. EXPERIMENTAL DATA

We have measured the transmission of $Al_2O_3:Mn^{3+}$ in the frequency range from 3 to 30 cm^{-1} as a function of applied magnetic fields up to 55 kG. The points in Fig. 3 are the positions of observed far-infrared absorption lines plotted as a function of applied magnetic field. The data were separated into ground-state transitions [Fig. 3(a)] and ex-

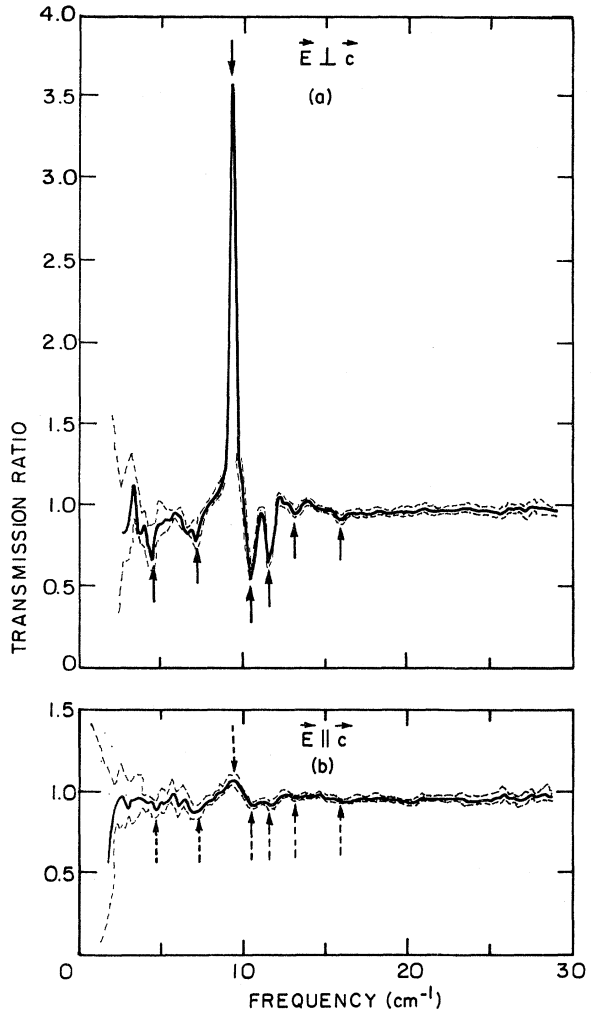

FIG. 2. Transmission ratios for sample S-18 at 4.2 K for two polarizations. The spectra in the numerators were measured in an applied field of 22.97 kG perpendicular to $\vec{c}$. The spectra in the denominators were measured in zero applied field. The dashed lines are plotted at ±1 standard deviation. In (a) the peak at 9.35 cm^{-1} is due to an absorption line in the zero-field denominator. The features at 4.45, 7.22, 10.55, 11.71, 13.19, and 15.90 cm^{-1} marked by solid arrows are due to absorption lines in the numerator. In (b) the positions of the features observed in (a) are marked by dashed arrows. These transitions are forbidden in the $\vec{E} \parallel \vec{c}$ polarization, and are seen due to imperfect polarization.

TABLE I. Sample data.

Sample	Source	Length (cm)	Mean diameter (cm)	$\vec{c}$	Analysis (% by weight) Mn	Cr	Fe
S-4	A. C. Pastore, Korad Corp.	1.5	0.8	∥	0.01	0.5	0.01
S-5	W. Brower, National Bureau of Standards	1.9	0.3	∥	0.001	< 0.001	0.001
S-14	Hrand Djevahirdjian S.A. (Switzerland)	2.5	1.0	∥	0.02	< 0.001	0.1
S-18	C. Sahagian, Air Force Cambridge Research Lab.	3.9	0.8	⊥	0.02	< 0.001	< 0.001

cited-state transitions [Fig. 3(b)] by measurement of the temperature dependence of the line strengths. The data for which the applied field was oriented parallel to the crystallographic $\vec{c}$ axis were measured using samples S-4, S-5, and S-14. The data for $\vec{H} \perp \vec{c}$ were measured using S-18.

Two absorption lines are observed to intersect zero field near 5 cm^{-1} in both the $\vec{H} \parallel \vec{c}$ and $\vec{H} \perp \vec{c}$ orientations. In the parallel-field case, the lines are degenerate at $H = 0$ with a frequency of 5.2 cm^{-1}. In the perpendicular-field case the modes intersect $H = 0$ at 4.5 and 5.2 cm^{-1}. Temperature dependence establishes that all of these modes are due to transitions from a singlet ground state. Furthermore, the temperature-dependence data show that the state which lies 4.5 cm^{-1} above the ground state is the lowest-lying excited state of the system. The transition to this state is therefore labeled $1 \rightarrow 2$. The two degenerate states which lie 5.2 cm^{-1} above the ground state in zero field are states 3 and 4. The $\vec{H} \parallel \vec{c}$ transitions are therefore labeled $1 \rightarrow 3$ and $1 \rightarrow 4$. The $\vec{H} \perp \vec{c}$ absorption line that intersects $H = 0$ at 5.2 cm^{-1} is either a $1 \rightarrow 3$ or a $1 \rightarrow 4$ transition. Comparison of model calculations based on these two possible assignments indicates that the transition is probably $1 \rightarrow 3$. The intensities of these transitions are field dependent, as indicated in Fig. 4. They have zero intensity at zero applied field, while at 50 kG, these lines dominate the observed spectra.

Two absorption lines are observed which intersect $H = 0$ at 9.35 cm^{-1}. These lines are also ground-state transitions and have been labeled $1 \rightarrow 5$ and $1 \rightarrow 6$. In zero field the degenerate $1 \rightarrow 5, 6$ line is the dominant absorption feature in the spectra of all the samples studied. The intensity of these lines decreases with field, as is shown in Fig. 4. In all three of the samples used for the $\vec{H} \parallel \vec{c}$ studies the $H = 0$ line was asymmetric with a linewidth (full width at half-peak-absorption coefficient) of 0.6 to 0.8 cm^{-1}, depending on the sample. In S-18, used for the $\vec{H} \perp \vec{c}$ studies, the $H = 0$ line was symmetric with a linewidth of 0.3 cm^{-1}. The linewidths are not temperature dependent below 20 K. We have not identified the mechanism responsible for broad lines in certain samples.

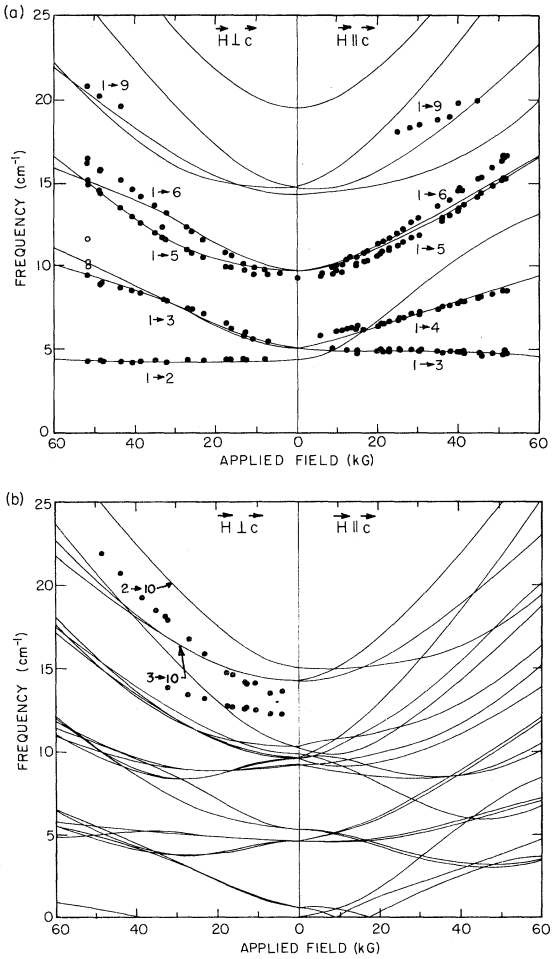

FIG. 3. Points are the positions of observed (a) ground-state and (b) excited-state transitions plotted as a function of applied magnetic field oriented parallel to $\vec{c}$ (right-hand side) and perpendicular to $\vec{c}$ (left-hand side). Transitions are labeld with the assigned initial and final states. The solid lines are calculated ground-state transitions in (a) and excited-state transitions in (b). In (b) only transitions arising from states 2, 3, and 4 are plotted.

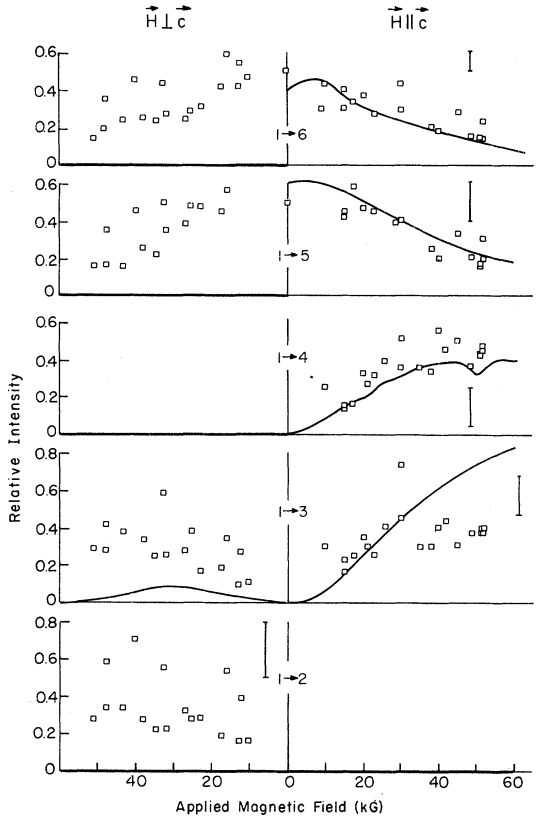

FIG. 4. Intensities of the lowest five ground-state transitions at 4.2 K plotted as a function of applied field. Intensities were normalized by the intensity of the $1 \rightarrow 5,6$ transition in zero field. The vertical bars indicate estimated errors in the determination of the normalized intensities. The solid lines are theoretical intensities at 4.2 K.

The weak ground-state transition labeled $1 \rightarrow 9$ is observable only at the highest available fields. This transition was observed only in the two samples with the greatest Mn concentration.

In the $\vec{H} \perp \vec{c}$ orientation (sample *S*-18) the two weak excited-state transitions shown in Fig. 3(b) were observed. These lines were only observed in the sample containing the largest total number of Mn ions. The separation between the two observed excited-state transitions is equal to the separation between the $1 \rightarrow 2$ and $1 \rightarrow 3$ transitions at all values of applied field. Thus, it is reasonable to suppose that the excited-state lines are due to transitions between the states 2 and 3 and some single higher-lying state. The best candidate for this higher-lying state is the singlet level 10. The lower excited-state transition in Fig. 3(b) is, then, $3 \rightarrow 10$, while the higher transition is $2 \rightarrow 10$. The temperature dependence of these lines seems to confirm this identification.

The shape of samples *S*-4, *S*-5, and *S*-14 was such that they were studied only with the incident radiation polarized perpendicular to the $\vec{c}$ axis. Sample *S*-18, however, is oriented so that both parallel and perpendicular polarization could be studied. A linear polarizer consisting of 10^3 gold strips per inch on a Mylar substrate was attached to this sample with rubber cement. Typical transmission ratios are displayed for the two polarizations in Figs. 2(a) and 2(b) for applied fields of 22.97 kG perpendicular to $\vec{c}$ at 4.2 K. The spectrum for $\vec{E} \parallel \vec{c}$ in Fig. 2(b) contains weak features which correspond to those in Fig. 2(a). However, these features may be explained by imperfect polarization arising from multiple reflections in the sample. To the accuracy of the experiment, these absorption lines are completely polarized. The three experimentally accessible combinations of orientation and polarization—$\vec{H} \parallel \vec{c}$, $\vec{E} \perp \vec{c}$; $\vec{H} \perp \vec{c}$, $\vec{E} \perp \vec{c}$; and $\vec{H} \perp \vec{c}$, $\vec{E} \parallel \vec{c}$—are sufficient to unambiguously assign the observed absorption lines to electric dipole transitions.

IV. THEORY

The JT effect is expected to play an important role in the states that we have studied. Several attempts have been made to calculate the lowest-lying vibronic states of Mn^{3+} and the isoelectronic species Cr^{2+} in Al_2O_3.[12-14] Because of the extreme complexity of the problem, however, these efforts have met with limited success. We have attempted to model the system with a purely electronic Hamiltonian with adjustable interaction strengths determined by empirically fitting the observed field-frequency curves in Fig. 3. We assume that the deviations of the interaction strengths from the values one would expect without a JT interaction measure the Ham quenching factors[15] of a more complete vibronic theory.

Our model Hamiltonian is the sum of crystal-field, spin-orbit, spin-spin, and Zeeman terms. Since hyperfine splittings are too small to be resolved in our experiments, we neglect them.

$$\mathcal{H} = V_{\text{xtal}} + V_{\text{so}} + V_{\text{ss}} + V_Z . \tag{1}$$

The crystal-field potential V_{xtal} consists of a cubic term, a trigonal distortion, and an inversion-breaking term. The cubic and trigonal fields are written using the usual spin operators,[16]

$$\begin{aligned} V_{\text{cubic}} &= -\tfrac{2}{3}B_4(O_4^o + 20\sqrt{2}O_4^3), \\ V_{\text{trig}} &= B_2^o O_2^o + B_4^o O_4^o, \end{aligned} \tag{2}$$

where the *B* coefficients are related to McClure's parameters[17]

$$\begin{aligned} Dq &= 12B_4 - \tfrac{14}{3}B_4^o, \\ v &= 9B_2^o + 80B_4^o, \\ v' &= \sqrt{2}(3B_2^o + 20B_4^o). \end{aligned} \tag{3}$$

A Hamiltonian consisting only of cubic and trigonal fields has D_{3d} symmetry. In order to correctly represent the splitting of the 9.35-cm^{-1} line in an applied field, the symmetry of our Hamiltonian must be no higher than C_3. We reduce the symmetry by adding an inversion-breaking term V_{ib}. Odd-order terms can occur in the Hamiltonian in the absence of inversion symmetry. Since these terms vanish within the ^5D manifold ($L=2$, $S=2$), they admix excited configurations into the ^5D state. It is important to consider such admixtures when computing transition probabilities, but they may be neglected when calculating the energies of the low-lying levels of the system. The only symmetry-allowed even-order term not already included in the crystal field is

$$A_4^3 \propto (1/2i)(Y_4^3 + Y_4^{-3}). \tag{4}$$

The dominant inversion-breaking term is, then,

$$V_{ib} = B_4^i A_4^3. \tag{5}$$

Within the ^5D manifold, the spin-orbit interaction may be written $V_{so} = \lambda \vec{L} \cdot \vec{S}$. The V_{ss} term,

$$V_{ss} = -\rho(\vec{L} \cdot \vec{S})^2, \tag{6}$$

contains contributions from two sources. The first is the usual spin-spin interaction which may be written in an L-S coupling scheme as[16]

$$-\rho[(\vec{L} \cdot \vec{S})^2 + \tfrac{1}{2}(\vec{L} \cdot \vec{S}) - \tfrac{1}{3}L(L+1)S(S+1)].$$

The second source is the admixture of excited terms (in particular, the ^3H term) of the $3d^4$ configuration through spin-orbit coupling. A typical contribution might be schematically written in the form

$$\sum_{^3H \text{ states}} \sum \frac{\langle {}^5D|\vec{L} \cdot \vec{S}|{}^3H\rangle\langle {}^3H|V_{xtal}|{}^3H\rangle\langle {}^3H|\vec{L} \cdot \vec{S}|{}^5D\rangle}{(E_{^5D} - E_{^3H})^2}.$$

Since these contributions are small, the approximation of including them in Eq. (6) seems justified. The Zeeman interaction is written $(k\vec{L} + 2\vec{S})\mu_B H$, where k is included to allow for covalency effects. A typical value of k is 0.8 for transition-metal ions in Al_2O_3.

The 25-dimensional Hamiltonian matrix of Eq. (1) was evaluated in terms of the seven adjustable parameters B_4, B_2^o, B_4^o, B_4^i, λ, ρ, and k using $3d^4(^5D)$ free-ion wave functions as a basis. Radial integrals were incorporated in the adjustable parameters. The schematic level diagram of Fig. 1 was verified by studying the general properties of the Hamiltonian as a function of the parameters. The splittings δ shown in Fig. 1(b) are given by[16]

$$\delta = 6(\rho + \lambda^2/10Dq).$$

The inversion-breaking parameter B_4^i has little effect on the zero field energy levels. With a finite magnetic field, it split 5 and 6, as expected. It also has large effects on the field dependence of the other energy levels. The orbital Zeeman effect is completely quenched within ^5E, the parameter k having no effect on the field dependence of the energy levels.

The adjustable parameters were determined by fitting the field-frequency data of Fig. 3 using a conventional least-squares procedure. It was found that good fits could not be achieved simultaneously for the ground- and excited-state data. A fit was attempted using the ground-state transitions alone, but there were more adjustable parameters than could be determined from the data. In order to obtain a fit, B_4 was fixed. This parameter, which measures the cubic field, is not expected to be quenched by a JT interaction and can be determined from optical data. Unfortunately, the value of B_4 is uncertain. Measurements by McClure[17] and Forman[18] suggest values of 160.4 and 142.1 cm^{-1}, respectively. Fits were obtained using a number of values of B_4 between 140 and 165 cm^{-1}. Although the parameters obtained differed for each value of B_4, the resultant energy-level diagrams were very similar. The parameters obtained using McClure's and Forman's values of B_4 are listed in Table II. Considering the uncertainty in B_4, our parameters are determined only to within 15%. Some results, however, are clear. The trigonal field and spin-orbit interactions are strongly quenched. The inversion-breaking term is small, typically several cm^{-1}. The parameter ρ is about 0.8 cm^{-1}.

The three most important results of the model are the values of v, λ, and ρ. Because of JT quenching, the trigonal-field parameter v has only 60–70% of its expected value. The spin-orbit coupling is very strongly quenched, having only about 10% of its free-ion value. Finally, the parameter ρ has an unexpectedly important role in the structure of the ^5E state. Since λ is so strongly quenched, $\delta \approx 6\rho$. The splittings δ, however, are the most obvious feature of the ^5E energy-level diagram. The parameter ρ is much larger than expected from a spin-spin interaction alone, suggesting that there is a considerable contribution to ρ from second-order spin-orbit coupling. This admixture of higher-lying terms has a particularly important role in determining the structure of the ^5E state.

V. COMPARISON WITH EXPERIMENT

The predicted ground-state transitions are shown as solid lines on Fig. 3(a). The fits to the $1 \rightarrow 2$, $1 \rightarrow 3$, and $1 \rightarrow 4$ transitions are excellent. We regard the fits to the $1 \rightarrow 5$ and $1 \rightarrow 6$ transitions to be satisfactory, considering the many approximations and simplifications made in the model. Predictions of the temperature dependence of the peak absorption coefficients of the ground-state transitions

TABLE II. Interaction parameters for $Al_2O_3:Mn^{3+}$

		Dq	v	v'	B_4	B_2^o	B_4^o	B_4^i	λ	ρ	k
Without JT		1947[a] 1727[b]	1950	600	160.4 142.1	173.7	−4.837		87[c]	0.18[d]	0.8
Theory	(e)	1946.4	1359.8	335.2	160.4	109.9	−4.634	−3.138	6.101	0.8074	•••
	(f)	1725.2	1234.8	298.6	142.1	99.0	−4.296	−2.805	6.059	0.8069	•••
Quenching factor	(e)		0.70	0.56		0.63	0.96		0.07		
	(f)		0.63	0.50		0.57	0.89		0.07		

[a]McClure (Ref. 17).
[b]Forman (Ref. 18).
[c]Free-ion value.
[d]Spin-spin interaction only.
[e]Calculation based on a value of 160.4 cm^{-1} for B_4.
[f]Calculation based on a value of 142.1 cm^{-1} for B_4.

were made using the theoretical level diagram and simple population arguments. The predicted temperature dependence agreed within experimental error limits with measurements made at seven temperatures between 1.3 and 20 K.

In order to compare theoretical and experimental line strengths, an extension of our model is required. Electric dipole transitions occur through configurational mixing. The lowest-lying configuration which can lead to the required mixing is the $3d^3 4p$ configuration. Ignoring term separations within $3d^3 4p$, we have admixed Slater determinantal wave functions of $3d^4(^5D)$ and $3d^3 4p$ using an interaction proportional to O_1^o. Point-charge-model calculations indicate that the O_1^o interaction is the largest allowed odd-order crystal-field interaction for the atomic configuration of Al_2O_3. Our resultant admixed wave functions were used to calculate electric dipole matrix elements for the $^5D_{\text{admixed}}$ states. These matrix elements were used with the eigenfunctions of Eq. (1) and the appropriate population factors to predict ground-state transition probabilities at 4.2 K.

In order to compare calculated transition probabilities with observed peak absorption coefficients, a normalization factor is required because the concentration of Mn^{3+} in our samples is not known. Spectrochemical analysis yields an estimate of the total Mn concentration in the sample, but provides no information on the distribution of Mn valence states. We chose to normalize the data in Fig. 4 to the strength of the 9.35-cm^{-1} line in zero field. The equivalent normalization factor for the theoretical transition probabilities is the sum of the probabilities of the $1 \rightarrow 5$ and $1 \rightarrow 6$ transitions in zero field. The normalized transition probabilities for the lowest five ground-state transitions are shown as the solid lines in Fig. 4. For $\vec{H} \parallel \vec{c}$ the model is seen to be in excellent agreement with experiment. For $\vec{H} \perp \vec{c}$, however, the model fails to account for the observed intensities. There could be several reasons for the discrepancy. We have included only one of the odd-order operators that could cause configurational mixing and have neglected mixing with the excited terms of the $3d^4$ configuration which could also be important. One might also expect that the JT interaction, which has not been explicitly included in our model, would affect the transition probabilities in a significant way.

A further confirmation of the ability of our model to describe the low-lying states of Mn^{3+} may be obtained by considering the acoustic-paramagnetic-resonance (APR) data of Anderson, Bates, and Jaussaud[5] (ABJ). In that paper, ABJ reported the observation of five APR lines in $Al_2O_3:Mn^{3+}$ at frequencies near 0.3 cm^{-1}, which they labeled B, D, E, F, and G. These lines are due to transitions between states 2, 3, and 4. In Fig. 5, the solid lines are the theoretical transition frequencies for the transitions between these three states as a function of applied field. Since level 2 crosses levels 3 and 4 in this orientation, transitions $3 \rightarrow 2$ and $4 \rightarrow 2$ are plotted as well as $2 \rightarrow 3$, $2 \rightarrow 4$, and $3 \rightarrow 4$. The points are the data of ABJ. We identify

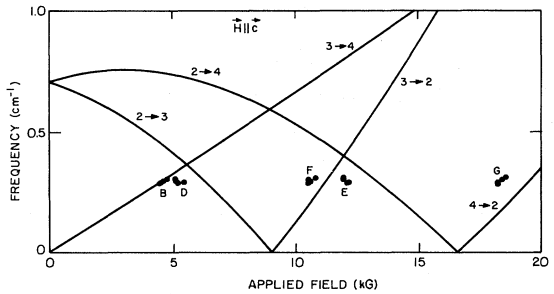

FIG. 5. Solid lines are theoretical low-lying excited-state transitions plotted as a function of applied field oriented parallel to $\vec{c}$. They are labeled by the initial and final states. The points indicate observed APR lines (Ref. 5), labeled as in that paper.

the APR line B as being due to $3 \rightarrow 4$. D, E, F, and G are due to transitions $2 \rightarrow 3$, $2 \rightarrow 4$, $3 \rightarrow 2$, and $4 \rightarrow 2$, respectively. In this field orientation the observable far-infrared transitions are $1 \rightarrow 3$ and $1 \rightarrow 4$. Transition $1 \rightarrow 2$ is forbidden. Hence, no information about the field dependence of level 2 in this field orientation was used to fit the model. The data of ABJ indicate, however, that the model correctly predicts the position of this level to within 0.1 cm^{-1}.

Although our model provides an excellent description of the ground-state transitions, it is not as successful with the excited-state transitions, $3 \rightarrow 10$ and $2 \rightarrow 10$. The theoretical excited-state transitions arising from states 2, 3, and 4 are indicated as solid lines in Fig. 3(b). Clearly there are serious discrepancies between theory and experiment. Level 10 is located about 2 cm^{-1} lower than our model predicts, and its energy depends less strongly on applied field than the model indicates. In addition, at temperatures above 10 K, the observed lines are much weaker than the predicted temperature dependence would indicate. It seems likely that a proper treatment of the JT interaction would reduce these discrepancies.

The simplest model of the JT interaction in Mn^{3+} is a cluster model in which the ^5E state interacts with an E-symmetry vibrational state of the cluster. From group-theoretic considerations

$$^5E_{\text{electronic}} \times E_{\text{phonon}} = {}^5E_{\text{vib}} + {}^5A_{\text{vib}} + {}^5A_{\text{vib}},$$

where the subscript vib stands for vibronic states. The JT interaction removes the degeneracy of these vibronic states. Our data clearly indicate that the $^5E_{\text{vib}}$ state is lowest.

This simple JT model could account for some of the discrepancies between our theory and the experiment. Level repulsion from the $^5A_{\text{vib}}$ states could lower the energy of level 10 and affect its field dependence, thus improving the poor fit for the observed excited-state transitions. In addition, including ten energy levels (two $^5A_{\text{vib}}$ states) at 25 cm^{-1} above the ground state greatly improves the fit to the measured temperature dependence of the excited-state transitions.

VI. γ-IRRADIATED RUBY

It has been suggested[19] that an important radiation-damage mechanism in ruby could be associated with the formation of Cr^{2+} and Cr^{4+} ions. Both of these ions are expected to have level splittings at far-infrared frequencies. Since Cr^{2+} is isoelectronic to Mn^{3+}, it is believed to have a similar level structure. Microwave studies of Cr^{4+} by Hoskins and Soffer[20] indicate that this ion should have a zero-field splitting of about 7 cm^{-1}.

The spectrum of a 15-cm-long crystal, whose $\vec{c}$ axis made an angle of 60° to the cylinder axis, showed weak absorption lines at 6.5 and 7.5 cm^{-1} in zero field at 4.2 K. In a field of 51 kG applied along the cylinder axis, only a single line at 4.5 cm^{-1} was observed. The zero-field lines were observed with a signal-to-noise ratio near 2, so that applied field splittings of these lines would not have been observed. After several days exposure to room lighting, the sample became optically bleached. Its color changed from red-orange to red and the far-infrared absorption lines were no longer observed. Since the available infrared data are poor, it is not possible to determine the ions responsible for the zero-field lines. The 4.5-cm^{-1} line in nonzero field would seem to have a field-dependent intensity and might therefore be assigned to Cr^{2+}.

It is known that the cubic field, spin-orbit, and spin-spin interactions of Cr^{2+} in typical environments are roughly two-thirds as strong as for Mn^{3+}. If we assume that all parameters of Cr^{2+} are two-thirds their value in Mn^{3+} and further assume that the quenching factors for the two ions are the same, then the resultant level diagram is qualitatively similar to Mn^{3+}. The energy of the zero field $1 \rightarrow 5, 6$ transition is 6.5 cm^{-1}. The $1 \rightarrow 2$ transition has an energy of 4 cm^{-1} for a field of 50 kG oriented at 60° with respect to $\vec{c}$. These results are undoubtedly fortuitous, but they suggest one possible interpretation of the data for γ-irradiated ruby. Comparison of this model with APR data[5] for Cr^{2+} yields rather poor agreement, as one would expect from such a crude estimate of model parameters.

If we assume that either the 6.5-cm^{-1} line or the 7.5-cm^{-1} line is due to Cr^{2+}, we may make a rough estimate of its concentration. If we assume that the transition probability per ion is the same for Cr^{2+} and Mn^{3+}, then by assuming that all of the Mn in sample S-18 is in the 3+ valence state and by comparing peak absorption coefficients and sample volumes we may obtain an upper limit of the Cr^{2+} concentration in our sample of γ-irradiated ruby. We find an upper limit of 5×10^{16} cm^{-3}. This represents only 1 part in 10^4 of the Cr in the crystal.

This estimate is much lower than usually quoted. Most estimates of Cr^{2+} concentration are made by assuming that the change in the Cr^{3+} EPR signal upon irradiation is directly proportional to the amount of Cr^{2+} formed.[21] The above estimate, however, suggests that the decrease in the EPR signal may be due to some other aspect of the damage mechanism and that Cr^{2+} formation is unlikely to be associated with the most important damage mechanisms in ruby.

We have studied several samples of Mg-doped ruby in the hope that Cr^{4+} formation would be favored through a change-compensation mechanism, but have been unable to observe any absorption lines.

ACKNOWLEDGMENTS

We would like to gratefully acknowledge very useful theoretical discussions with C. A. Bates, L. J. Challis, and L. Falicov. We also acknowledge extensive discussions with R. A. Forman, who shared with us the results of unpublished measurements on both the $Al_2O_3:Mn^{3+}$ and the γ-irradiated-ruby systems. We are indebted to R. A. Forman and B. Soffer for providing samples and to G. Shalimoff for the spectrochemical analysis. This work was supported in part by the U. S. Energy Research and Development Administration.

[1]A. M. deGöer and B. Dreyfus, Phys. Status Solidi 22, 77 (1967).
[2]L. J. Challis and A. M. deGöer, Phys. Lett. A 31, 463 (1970).
[3]M. Locatelli, P. Jaussaud, and A. M. deGöer, C. R. Acad. Sci. B 270, 620 (1970).
[4]R. S. Anderson, R. G. Brabin-Smith, and V. W. Rampton, J. Phys. C 3, 2379 (1970).
[5]R. S. Anderson, C. A. Bates, and P. C. Jaussaud, J. Phys. C 5, 3397 (1972).
[6]R. S. Anderson, C. A. Bates, P. C. Jaussaud, and V. W. Rampton, J. Phys. C 5, 3414 (1972).
[7]R. L. Aurbach, P. L. Richards, and R. A. Forman, Bull. Am. Phys. Soc. 18, 1572 (1973).
[8]J. H. M. Stoelinga, P. Wyder, L. J. Challis, and A. M. deGöer, J. Phys. C 6, L 486 (1973).
[9]R. R. Joyce and P. L. Richards, Phys. Rev. 179, 375 (1969).
[10]R. R. Joyce, Ph. D. thesis (University of California, Berkeley, 1970) (unpublished).
[11]D. H. Martin and E. Puplett, Infrared Phys. 10, 105 (1969).
[12]C. A. Bates and J. M. Dixon, J. Phys. C 2, 2209 (1969).
[13]C. A. Bates and J. M. Dixon, J. Phys. C 2, 2225 (1969).
[14]C. A. Bates, P. C. Jaussaud, and W. Smith, J. Phys. C 6, 898 (1973).
[15]F. S. Ham, in *Electron Paramagnetic Resonance*, edited by S. Geschwind (Plenum, New York, 1972).
[16]A. Abragam and B. Bleaney, *Electron Paramagnetic Resonance of Transition Metal Ions* (Clarendon, Oxford, England, 1970).
[17]D. S. McClure, J. Chem. Phys. 36, 2757 (1962).
[18]R. A. Forman (private communication).
[19]For example, D. R. Mason, and J. S. Thorp, Proc. Phys. Soc. Lond. 87, 49 (1966); T. Maruyama and Y. Matsuda, J. Phys. Soc. Jpn. 19, 1096 (1964).
[20]R. H. Hoskins and B. H. Soffer, Phys. Rev. 133, A490 (1964).
[21]For example, G. E. Arkhangelskii, Z. L. Morgenshtern, and V. B. Neustruev, Phys. Status Solidi 22, 289 (1967); T. Maruyama, Y. Matsuda, H. Kon, and H. Yonemitsu, J. Phys. Soc. Jpn. 18, 315 (1963); A. F. Forestieri and H. H. Grimes, NASA Technical Note TN D-3379, 1966 (unpublished).